Cellulose (2020) 27:8695–8708
https://doi.org/10.1007/s10570-020-03366-5

ORIGINAL RESEARCH

Cellulose nanofibers electrospun from aqueous conditions

Hui Zhang · Yan Liu · Sisi Cui · Yifa Zhou · Junli Hu · Jiangang Ma · Yichun Liu

Received: 12 January 2020 / Accepted: 23 July 2020 / Published online: 4 August 2020

Abstract Electrospun cellulose nanofibers are promising biomaterials but are suffering from the use of unfavorable organic solvents during the electrospinning process. In this manuscript, we used the periodate oxidation—adipic acid dihydrazide crosslinking strategy to fabricate electrospun cellulose nanofibers. Periodate oxidation of cellulose generated water soluble aldehyde cellulose, which thus allowed for the electrospinning in aqueous solution and avoided the use of unfavorable organic solvents. The following crosslinking with adipic acid dihydrazide made the nanofibers water resistant. The results show that the prepared cellulose nanofiber mats show moderate wet mechanical strength around 1 MPa, are able to absorb water equal to 30 times of their own weight, can degrade gradually by hydrolysis, and are cytocompatible. These cellulose nanofibers are expected to find applications in biomedical fields such as wound healing and tissue regeneration.

H. Zhang · Y. Liu · J. Hu · J. Ma (✉) · Y. Liu
Key Laboratory of UV-Emitting Materials and Technology (Northeast Normal University), Ministry of Education, Changchun 130024, Jilin, China
e-mail: majg@nenu.edu.cn

S. Cui · Y. Zhou
School of Life Sciences, Northeast Normal University, Changchun 130024, Jilin, China

J. Hu (✉) · J. Ma · Y. Liu
National Demonstration Centre for Experimental Physics Education, Northeast Normal University, Changchun 130024, Jilin, China
e-mail: hujl100@nenu.edu.cn

Graphic abstract

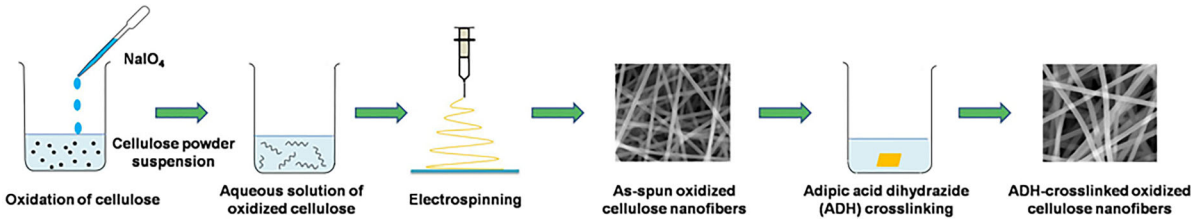

Keywords Cellulose · Nanofiber · Electrospinning · Crosslinking

Introduction

Cellulose, a linear homopolysaccharide composed of β-1,4-linked D-glucopyranose, is the most abundant biomass in nature and the most attractive natural materials in human life (Morán et al. 2008). Cellulose and its derivatives have a long application history in medical fields, from the very traditional cotton gauzes to the modern hemostatic powders and wound dressings (Cullen et al. 2002; Hart et al. 2002; Gabriel et al. 2020; Wu et al. 2017). Nanocellulose refers to cellulose materials with one or more dimensions in nanoscale. There are different types of nanocellulose, cellulose whisker, micro fibrillated cellulose, bacterial cellulose, and electrospun cellulose nanofibers (Klemm et al. 2011). Comparing with the other three types of nanocellulose, electrospun cellulose nanofibers have unique structural advantages for biomedical applications. Nanofibers of various surface morphologies, structures, or orientations were able to be fabricated by tuning the experimental setup and parameters during the electrospinning process, to satisfy the needs of various biomedical applications (Huang et al. 2003; Schiffman and Schauer 2008). The unique nonwoven nanofibrous structure generated by electrospinning also benefits biomedical applications as wound dressings and tissue engineering scaffolds (Kenawy et al. 2002; Khil et al. 2003; Kishan and Cosgriff-Hernandez 2017; Matthews et al. 2002). Electrospun cellulose nanofibers thus were used to carry active reagents such as photosensitizers, antibacterial or magnetic nanoparticles or conductive polymers, and applied for wound healing, tissue regeneration and other biomedical situations (Dong et al. 2018; Hou et al. 2016; Phan et al. 2019).

Due to the poor solubility of cellulose in water and common organic solvents, electrospun cellulose nanofibers are usually prepared through two approaches. One is firstly electrospinning the solution of cellulose derivatives in organic solvents, mostly the solution of cellulose acetate in acetone-containing solvents, and then regenerating cellulose nanofibers by hydrolysis treatments (Du and Hsieh 2009; Frenot et al. 2007; Frey 2008; Han et al. 2008). The other is electrospinning cellulose from its solution in good solvents, such as N-methylmorpholine-N-oxide (Kim et al. 2006; Kulpinski 2005; Magalhães et al. 2009), LiCl/dimethylacetamide (Frenot et al. 2007; Kim et al. 2006), and ionic liquids (Quan et al. 2010; Viswanathan et al. 2006; Xu et al. 2008). Both approaches are using organic solvents for electrospinning, which are toxic, expensive, or hard to remove from the nanofibers (Phan et al. 2019; Vallejos et al. 2012). The high cost and the possible toxic effects of the organic solvents limited the applications of the cellulose nanofibers in biomedicine.

Our group has previously developed a periodate oxidation—adipic acid dihydrazide (ADH) crosslinking strategy for the preparation of polysaccharide nanofibers. In this approach, polysaccharides are firstly oxidized with periodate to generate aldehyde groups in their molecular chains. The aldehyde polysaccharides are electrospun from their aqueous solutions and then crosslinked with ADH. A number of water soluble polysaccharides such as pectin, starch, and konjac glucomannan were fabricated into electrospun nanofibers through this approach, showing excellent water resistance and biocompatibility, and of high biomedical application potential (Chen et al. 2018; Lv et al. 2019; Zhang et al. 2019). In this manuscript, we applied this strategy to cellulose, the water insoluble polysaccharide, in view that periodate

oxidation of cellulose generates water soluble aldehyde cellulose, thus allowing for the electrospinning in aqueous solution and avoiding the use of unfavorable organic solvents. The results show that the prepared cellulose nanofibers show moderate mechanical strength, excellent water uptake ability and enhanced degradability, which benefit their applications in biomedical fields.

Materials and methods

Materials

Cellulose micropowders (size = 50 μm), ADH, hydroxylamine hydrochloride, methyl orange and poly(ethylene oxide) (PEO, Mv = 5000 kDa) were purchased from Aladdin Reagents (Shanghai, China). Triton X-100 and 3-(4,5-Dimethyl-2-thiazolyl)-2,5-diphenyl-2-H-tetrazolium bromide (MTT) were obtained from Dingguo Biotech (Beijing, China). Sodium periodate ($NaIO_4$) was purchased from Xilong Chemicals (Guangzhou, China). Dimethyl sulfoxide (DMSO) was from Tianjin Kemiou Chemical Reagent (Tianjin, China). All other chemicals were purchased from Sinopharm Chemical Reagent Beijing (Beijing, China). Deionized water was supplied by our laboratory. Murine L929 fibroblast cells were purchased from American Type Culture Collection.

Periodate oxidation of cellulose

Cellulose micropowders were mixed with $NaIO_4$ solution. The concentration of cellulose in the suspensions was 2%. The molar ratio between $NaIO_4$ and the anhydroglucose (AGU) units in cellulose was set at 30:100, 60:100, 90:100, 120:100, respectively. The pH of the suspensions was adjusted to 4.0 with 1 M HCl. The solutions were magnetically stirred in darkness at ambient temperature (20–25 °C) for 72 h. After the reactions, the mixtures were centrifuged at 10,000 rpm for 30 min. The supernatants were dialyzed against plenty of water and then freeze-dried, giving the solution fractions of oxidized cellulose (OC-S). The precipitates were washed with water, re-centrifuged, and freeze-dried. These oxidized cellulose powders (OC-P-0) were mixed with water (20 mL water per gram powders) and refluxed with an oil bath (130 °C) for 4 h. After cooling to room temperature, the undissolved residues were removed by centrifugation at 10,000 rpm for 30 min, and the supernatants were lyophilized, giving the powder fractions of oxidized cellulose (OC-P). The content of aldehyde groups and molecular weight of oxidized celluloses were determined as previously (Chen et al. 2018; Lv et al. 2019; Zhang et al. 2019).

Electrospinning of oxidized cellulose

The oxidized celluloses (OCs, including OC-Ps and OC-Ss) were dissolved homogeneously with PEO, Triton X-100 and DMSO in water to reach a total polymer concentration of 7.5%, an oxidized cellulose/PEO mass ratio of 80:20, a Triton X-100 concentration of 1.0 wt%, and a DMSO concentration of 5.0 wt%, respectively. The solutions were electrospun at ambient temperature with a spinneret diameter of 0.5 mm, a flow rate of 0.01 mL/min and a positive high voltage of 10 kV, and nanofiber mats were collected at a distance of 20 cm away from the spinnerets.

Crosslinking of electrospun oxidized cellulose nanofibers with ADH

The electrospun oxidized cellulose nanofibers (20 mg) were soaked in ADH solutions (50 mmol/L, 20 mL) in ethanol/water mixture solvent (80/20 V/V) for 8 h at ambient temperature and under moderate shaking (100 rpm). The crosslinked nanofibers were washed with plenty of water, ethanol and chloroform sequentially, and vacuum dried.

Characterization

Morphology

The morphologies of the samples were observed through a scanning electron microscope (SEM, XL-30 ESEM FEG, Micro FEI Philips) at an acceleration voltage of 20 kV. The samples were placed on sample stages with conductive tapes and sputter-coated with a thin layer of gold before measurements.

Chemical composition and crystallization

The Fourier transform infrared (FTIR) spectra were collected with a FTIR spectrometer (iS10, Thermo Scientific Nicolet) equipped with a photomultiplier

detector. The samples were homogeneously mixed with potassium bromide at a weight ratio of 1:100 and pressed into tablets. Spectra were obtained by recording 48 scans between 2000 and 800 cm^{-1} with a resolution of 4 cm^{-1}. The X-ray diffraction (XRD) patterns were characterized by an X-ray diffractometer (Rigaku, D/max-2500) using Cu Kα radiation (λ = 1.541 Å) operating at 40 kV and 30 mA. Scans were carried out in range of 10°–60° with a step size of 0.02° and a speed of 2°/min.

Mechanical property

Maximum tensile strength of the nanofiber mats was determined with a Universal Material Testing Machine (zwickiLine Z1.0TN, Zwick/Roell). The mats with a thickness of approximately 0.05 mm were cut into a dimension of 6 mm × 50 mm, wet with simulated body fluid (SBF) and drawn at a rate of 1 mm/min by two clamps with an initial distance of 4 cm. Maximum tensile strength was calculated from the stress–strain curves. Three parallel samples were tested.

Hydrophilicity and water uptake ability

To examine the hydrophilicity of the nanofiber mats, the nanofiber mats were spread on glass microslides. A 2 μL drop of water was dropped onto each nanofiber mat through a micropipette needle. Videos were recorded until the drop was completely absorbed by the nanofiber mat.

For water uptake ability tests, nanofiber mats (M_1 mg) were immersed in SBF at 37 °C for 30 min, and then hung with a tweezer for 30 s, and then weighed (M_2 mg). Afterwards, the above nanofiber mats with absorbed SBF were centrifuged at 1200 rpm for 15 min and weighed again (M_3 mg). The total uptake ability of the nanofiber mats was calculated as $(M_2 - M_1)/M_1$. The uptake ability of the fibers and the pores between the fibers was calculated as $(M_3 - M_1)/M_1$ and $(M_2 - M_3)/M_1$, respectively.

In vitro degradation

The nanofibers (10 mg) were placed into SBF (10 mL) and incubated at 37 °C. At the desired time points, the fibers were taken out and washed with plenty of water, ethanol and chloroform sequentially, and vacuum dried. The mass of the nanofibers was weighed with a balance with an accuracy of 0.01 mg (MS105DU, Mettler-Toledo) and the morphologies of the nanofibers were observed with SEM. Three parallel samples were tested.

Biocompatibility

Murine L929 fibroblast cells were used to investigate the biocompatibility of the nanofibers. The nanofibers (20 mg) were soaked in Dulbecco's modified Eagle's medium (DMEM, 2 mL) at 37 °C for 24 h to generate leachates. The cells were seeded in 96-well plates at a density of 3000 cells/well, and cultured in DMEM with 10% fetal calf serum for 24 h at 37 °C in a humidified atmosphere containing 5% CO_2. The leachates of the nanofibers were then added to the cells (n = 5). After culture at 37 °C for another 24 h, the viabilities of the cells were tested with MTT assay.

Results and discussion

Periodate oxidation of cellulose

For the oxidation of cellulose, cellulose micropowders were suspended in $NaIO_4$ solution for 72 h. The oxidation of cellulose occurred on the interface between cellulose micropowders and $NaIO_4$ solution. The oxidized cellulose might stay on micropowders or dissolve into solution if they achieved sufficient water solubility after oxidation. After the reaction, we collected micropowders (OC-P-0), dissolved them with boiling water and then freeze dried them, obtaining the powder fraction of oxidized cellulose (OC-P). In the meanwhile, we collected the solution, dialyze against water and freeze dried it, obtaining the solution fraction of oxidized cellulose (OC-S).

In order to control the oxidation degree of cellulose, we kept the amount of cellulose micropowders constant and changed the amount of the input $NaIO_4$. As shown in Fig. 1, as the molar ratio between $NaIO_4$ and the AGU units in cellulose increased, the yield of OC-P decreased almost linearly (Fig. 1a, black line) and that of OC-S increased linearly (Fig. 1b, black line), indicating that at the high $NaIO_4$ amount more oxidized cellulose dissolved into solution. As the $NaIO_4$/AGU molar ratio increased from 30 to 120%, the oxidation degree of OC-P increased almost

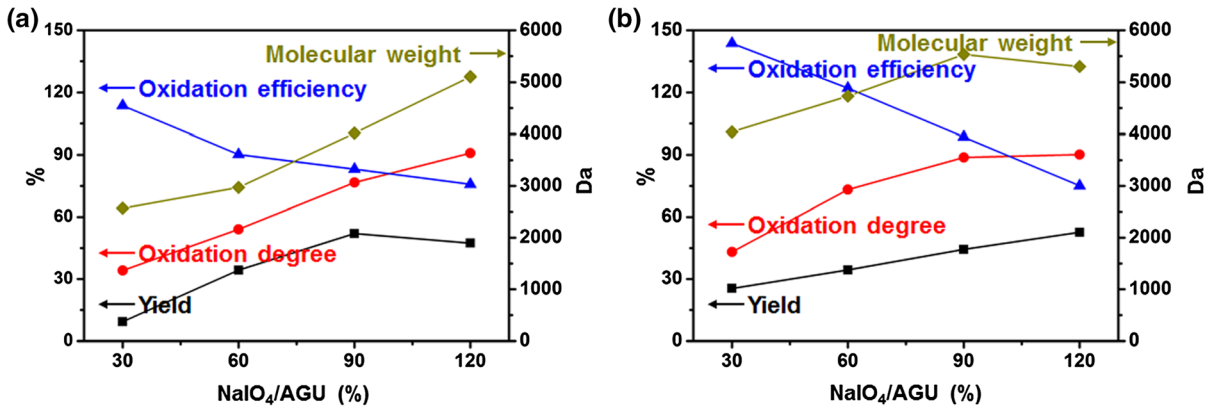

Fig. 1 Dependence of the yield, oxidation degree, oxidation efficiency and molecular weight of OC-P (**a**) and OC-S (**b**) on $NaIO_4$/AGU molar ratio

linearly from 34 to 91% (Fig. 1a, red line). The oxidation degree of OC-S also increased with the increase of $NaIO_4$/AGU molar ratio (Fig. 1b, red line). At the $NaIO_4$/AGU molar ratio between 30 and 90%, the oxidation degree of OC-S was 15–35% higher than that of OC-P, suggesting that more heavily oxidized cellulose tended to dissolve into water. At the $NaIO_4$/AGU molar ratio of 120%, the oxidation degree of OC-S was comparable with that of OC-P, probably because that most of the AGU units in cellulose have been oxidized in this case.

The oxidation efficiency of cellulose decreased with the increase of $NaIO_4$/AGU ratio (Fig. 1a, b, blue lines). At low $NaIO_4$/AGU ratio of 30% and 60%, efficiencies higher than 100% (up to ~ 150%) were obtained. As the $NaIO_4$/AGU ratio increased to 120%, the oxidation efficiency decreased to 75%. The oxidation of cellulose is a heterogeneous reaction. This is different from the common homogeneous oxidation of water soluble polysaccharides such as pectin (Chen et al. 2018) and konjac glucomannan (Zhang et al. 2019). We thus should examine the process of heterogeneous oxidation of cellulose carefully. In this process, it should be hard for the periodate ions to enter the inside of the cellulose powders. Initially, the oxidation reaction was more likely to be limited to the surface of the powders. When the cellulose molecules on the surface of the powders were oxidized to a certain extent and achieved sufficient water solubility, they detached from the surface and dissolved in the aqueous solution. Thereafter, a portion of periodate came to the new surface and reacted with the cellulose molecules therein, and another portion of periodate reacted with the dissolved cellulose molecules in the solution. These reactions continued until completion. We should also mention that when the powders after oxidation (OC-P-0) were heated in boiling water, in most cases part of them was not dissolvable and discarded. Only the water soluble part was recovered by lyophilization, forming OC-P portion. The recovery efficiency is 12.5%, 52.2%, 93.4% and 100% for the $NaIO_4$/AGU ratio of 30%, 60%, 90% and 120%, respectively. Therefore, the local $NaIO_4$/AGU ratio on powder surface or solution might exceed the appointed values. It is thus not surprising that the oxidation efficiency exceeded 100% in some cases. Several other groups have done the oxidation of cellulose at $NaIO_4$/AGU ratio of 125% or 130% under similar conditions. They collected the powder portion and found that the oxidation efficiency was ranged between 62 and 72%, which is comparable to our results at $NaIO_4$/AGU ratio of 120% (Kim et al. 2004; Liu et al. 2017; Münster et al. 2017).

Native cellulose has a molecular weight of thousands kDa. By contrast, the molecular weights of all OC-Ps and OC-Ss are below 10 kDa. These results indicate that severe depolymerization occurred during oxidation. The depolymerization of polysaccharides during the periodate oxidation process was observed widely in our previous work (Chen et al. 2018; Lv et al. 2019; Zhang et al. 2019). The severe depolymerization during the oxidation process of cellulose powder may also relate to the high local $NaIO_4$/AGU ratio as discussed above. The slight increase of apparent molecular weight with oxidation degree is perhaps

caused by more hemiacetal or acetal formation at higher oxidation degree (Fan et al. 2001).

The OC-P-0 s, OC-Ps and OC-Ss were indexed with their actual oxidation degree in the following text.

It is well known that TEMPO preferably oxidizes the amorphous regions of cellulose (Saito and Isogai 2004). In order to examine where the periodate oxidation most readily occurs, we measured the morphologies, sizes and crystallization patterns of the native and oxidized cellulose powders with SEM and XRD, respectively. The results are shown in Fig. 2. Native cellulose powders are rod-shaped, with a length of 50–150 μm and a diameter of 10–30 μm (Fig. 2a). After oxidation and as the oxidation degree increased, the cellulose powders first decreased their size, and then changed their morphology to irregular and flocculent shapes. These results suggest that the oxidation of cellulose started from the surface of the powders and proceeded into their interior. Native cellulose powders have three diffraction peaks at 16.0°, 22.6°, and 34.5° (Fig. 2b), which is a typical cellulose I diffractogram (French 2014). The intensity of these peaks decreased after oxidation and as the oxidation degree increased, which implies that the crystalline regions of the cellulose powders have been oxidized. Similar results have been reported previously (Kim et al. 2000; Münster et al. 2017). Therefore, for cellulose, periodate oxidation and TEMPO oxidation occurs at different regions. TEMPO oxidation occurs mostly on the amorphous regions of cellulose, generating products of increased

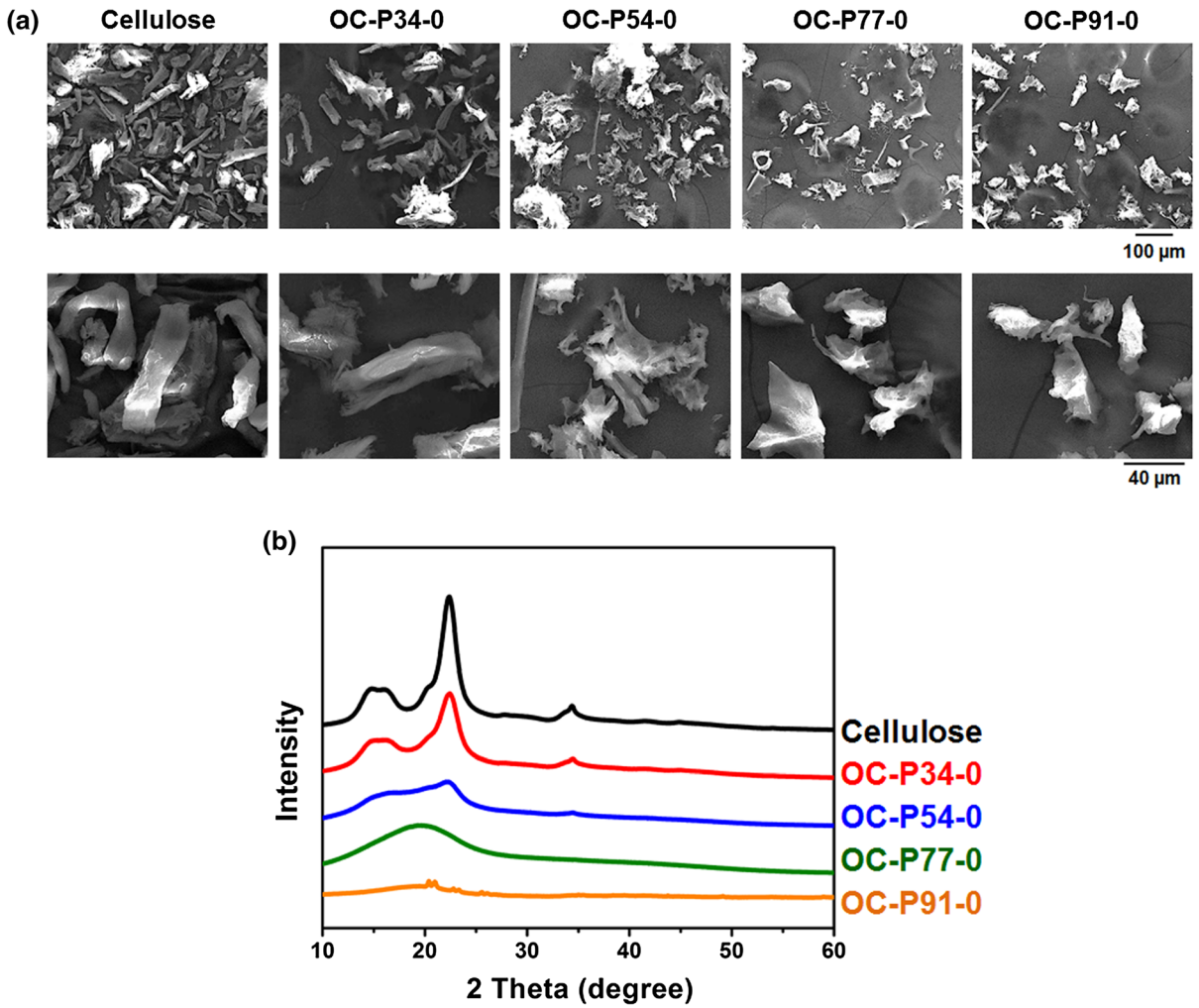

Fig. 2 SEM (**a**) and XRD (**b**) of the native and oxidized cellulose powders

crystallinity. Periodate oxidation perhaps occurs more on crystalline regions, and thus generates products of decreased crystallinity.

Electrospinning of oxidized cellulose and ADH crosslinking

All the oxidized celluloses (OCs, including OC-Ps and OC-Ss) are water soluble, and thus their nanofibers could be electrospun at aqueous conditions. As shown in Fig. 3, all OCs were capable of forming nanofibers with smooth surface and uniform size. The electrospun OC nanofibers were then crosslinked with ADH. After crosslinking, the nanofibers retained good nanofibrous morphology and smooth surface. There were no fusions between nanofibers. The average diameter of the as-spun OC-P34, OC-P54, OC-P77 and OC-P91 is 833 nm, 531 nm, 491 nm, and 303 nm, respectively. The fiber diameter decreased with the increase of oxidation degree. After crosslinking, the fiber diameter increased more or less. The diameter of the crosslinked OC-P34, OC-P54, OC-P77 and OC-P91 fibers is 855 nm, 715 nm, 654 nm, and 598 nm, respectively. There might be two things that occurred during the crosslinking process and changed the size of the fibers. One is the removal of electrospinning aiding reagents. The as-spun fibers contained PEO and Triton X-100. The crosslinking and the subsequent washing process removed PEO and Triton X-100 from the fibers, which might have reduced the fiber size. The other is the introduction of the ADH residues. During the crosslinking process, ADH reacted with the aldehyde groups of the oxidized cellulose and chemically bound in/onto the fibers, which could cause the increase of the fiber size. The two factors together determined the final fiber size. The eventual increase of fiber size after crosslinking probably suggests that the introduced ADH in nanofibers was at very high level and it over compromised the lost PEO and Triton X-100. The diameter of the as-spun and crosslinked OC-S fibers falls between 380–920 and 590–1730 nm, respectively, which are to some extent larger than the corresponding OC-P fibers, while similar dependences of fiber diameter on oxidation degree and crosslinking treatment were observed.

Chemical composition and crystallization

The chemical composition of the fibers was characterized by FTIR (Fig. 4). In comparison with native cellulose, both OC-S73 and OC-P77 show a new peak at 1730 cm^{-1}, assigning to the C = O stretching vibration of aldehyde groups (Fig. 4a, b, red line). Native cellulose inherently presents a small absorption peak at 890 cm^{-1} (Fig. 4a, b, black line) due to the inter- or intra-molecular hemiacetal groups. OC-P77 and OC-S73 have a much stronger absorption band at 890 cm^{-1}, probably because that part of the aldehyde groups generated by oxidation reacted with the adjacent hydroxyl groups and formed acetal or hemiacetal groups. These results prove that aldehyde groups were introduced by periodate oxidation. OC-

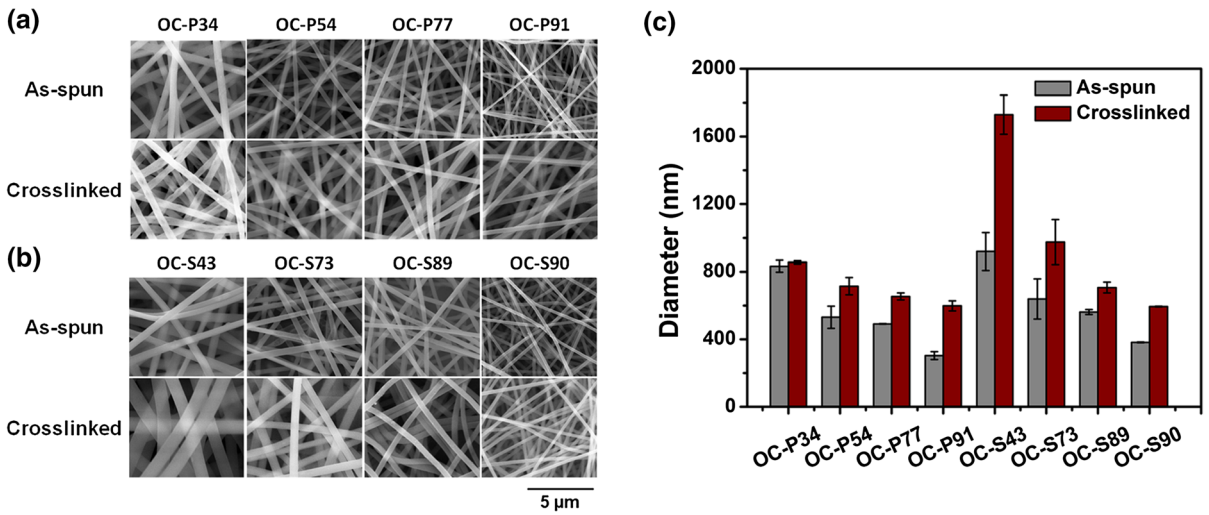

Fig. 3 SEM images (**a**, **b**) and size (**c**) of the as-spun and ADH-crosslinked OC-P and OC-S nanofibers

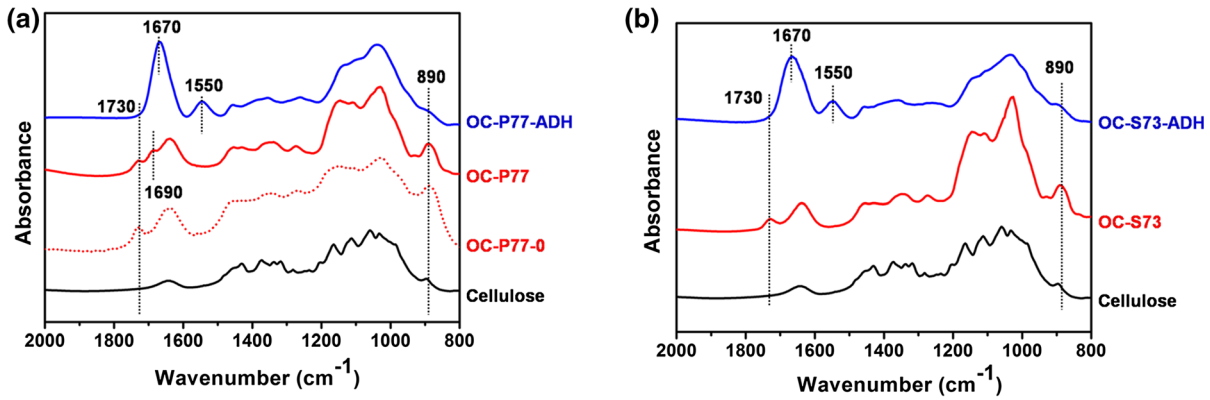

Fig. 4 (**a**) FTIR spectra of native cellulose, oxidized cellulose powders (OC-P77-0), OC-P77 and ADH-crosslinked OC-P77 nanofibers (OC-P77-ADH); (**b**) FTIR spectra of native cellulose, OC-S73 and ADH-crosslinked OC-S73 nanofibers (OC-S73-ADH)

P77 shows an additional peak at 1690 cm^{-1}, which is possibly the C = C stretching vibration of enol tautomerized from aldehydes after heating in boiling water, since the oxidized powders without being heated do not show this absorption (Fig. 4a, OC-P73-0, red dotted line). In the spectra of ADH-crosslinked OC-P77 and OC-S73 nanofibers (OC-P77-ADH and OC-S73-ADH, respectively, Fig. 4a, b, blue lines), there are no aldehyde peaks at 1730 cm^{-1} and the hemiacetal peak at 890 cm^{-1}, but appear new peaks at 1670 cm^{-1} and 1550 cm^{-1} attributing to the C = O stretching and the N–H bending of amide groups, respectively. These results indicate that ADH consumed the aldehyde groups and generated hydrazone bonds, and the crosslinking of oxidized cellulose was successful.

Figure 5 shows the XRD patterns of OCs and ADH-crosslinked OC nanofibers. Unlike the oxidized cellulose powders (Fig. 2b, OC-P-0), all OC-P samples only have a very broad maximum around 18.0° and all the typical cellulose I diffractogram disappears. These results demonstrate that the crystallization of cellulose has further been fully disrupted by the subsequent heating of the oxidized powders with boiling water. All OC-S samples also only have a very broad maximum around 18.0°. $NaIO_4$ attacked the C2–C3 bonds of AGU units (Leguy et al. 2018; Yan et al. 2019) and glycosidic bonds between the units in cellulose molecular chains (Fig. 1), causing the open of some AGU rings and broke of some glycosidic bonds. The oxidized cellulose with disrupted structure probably has lost their ability to pack orderly. The disruption of the crystallization is crucial for cellulose to achieve water solubility and realize the electrospinning in aqueous conditions. The ADH-crosslinked

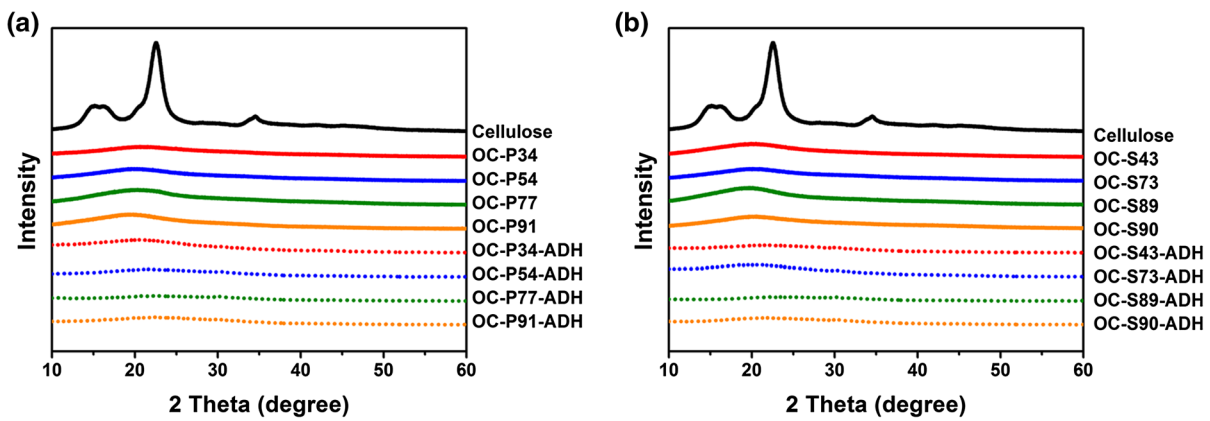

Fig. 5 X-ray diffraction patterns of native cellulose, oxidized cellulose, and ADH-crosslinked oxidized cellulose nanofibers

OC nanofibers also show no diffraction bands, indicating their completely amorphous state.

Mechanical property

The mechanical properties of the wet cellulose nanofiber mats are shown in Fig. 6. Overall, their tensile strength falls between 0.15 and 1.11 MPa. The tensile strength of ADH-crosslinked OC-P34, OC-P54, OC-P77 and OC-P91 fiber mats are 0.87 MPa, 0.62 MPa, 1.11 MPa, and 0.60 MPa, respectively. For ADH-crosslinked OC-S fiber mats, as the oxidation degree increased from 43 to 73%, the tensile strength increased from 0.15 MPa sharply to 0.97 MPa, and as the oxidation degree increased further to 89% and 90%, the tensile strength of the fiber mats decreased to 0.23 MPa gradually. OC-P77-ADH and OC-S73-ADH fiber mats have the highest strength around 1 MPa. This strength is moderate and can satisfy the needs of some biomedical applications (Khan et al. 2000; Zaman et al. 2011).

Hydrophilicity and water uptake ability

OC-P-ADH and OC-S-ADH nanofiber mats exhibit different hydrophilicity and kinetics of water uptake (Fig. 7). When water was initially dripped, OC-P-ADH and OC-S-ADH nanofiber mats showed different initial water contact angles, 92°, 86°, 83°, and 70° for OC-P34-ADH, OC-P54-ADH, OC-P77-ADH, and OC-P91-ADH nanofiber mats (Fig. 7a), and 69°, 64°, 53°, and 50° for OC-S43-ADH, OC-S73-ADH, OC-S89-ADH, and OC-S90-ADH nanofiber mats (Fig. 7b). All nanofiber mats completely absorbed water droplets within 1 s. The initial contact angle of the fiber mats gradually decreased as the oxidation degree increased, indicating the increased hydrophilicity. The initial contact angle of OC-P-ADH fiber mats is generally higher than that of OC-S-ADH fiber mats, suggesting that OC-S-ADH fiber mats are more hydrophilic than the corresponding OC-P-ADH fiber mats.

Oxidation degree seems to be a governing factor affecting the hydrophilicity of the nanofiber mats. For both OC-P and OC-S series, the higher the oxidation degree, the higher the hydrophilicity, the lower the initial contact angle. The effect of oxidation degree to some extent also leads to the lower initial contact angle of OC-S-ADH nanofiber mats than the corresponding OC-P-ADH ones (the ones produced at the same $NaIO_4$/AGU ratio) since OC-Ss have higher oxidation degrees than the corresponding OC-Ps (Fig. 1). Fiber size may also affect the hydrophilicity of the mats. OC-S-ADH fibers have a larger diameter than the corresponding OC-P-ADH fibers, especially at low $NaIO_4$/AGU ratio (Fig. 3c). As a result, OC-S-ADH fiber mats have larger pore sizes, lower porosity, and fewer air bubbles between fibers. Water drops can enter into the pores of between OC-S-ADH fibers more quickly. This might also to some extent contribute to the lower initial contact angle of the OC-S-ADH nanofiber mats.

The cellulose fiber mats are able to absorb aqueous solution. The nanofibers themselves can absorb

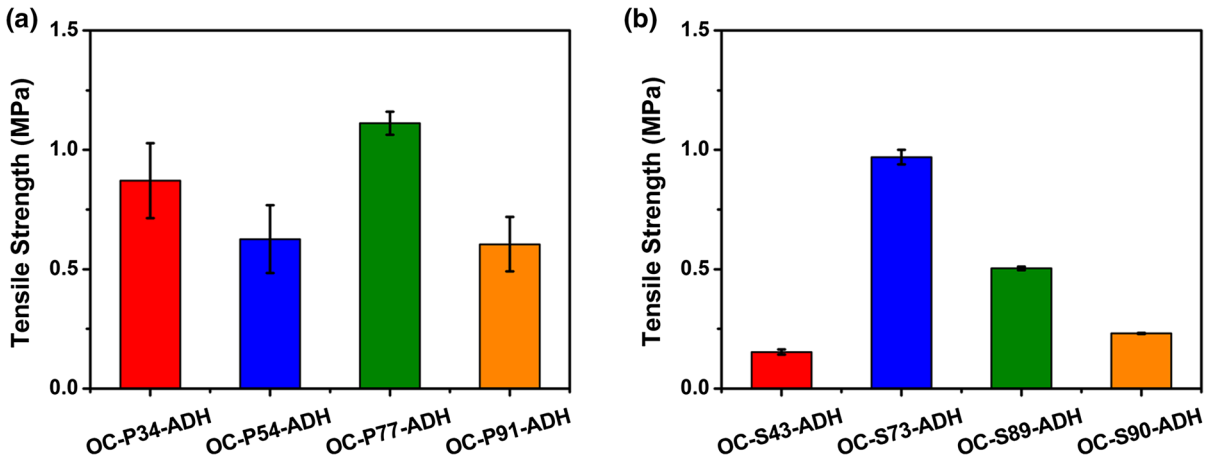

Fig. 6 The tensile strength of the prepared cellulose nanofiber mats

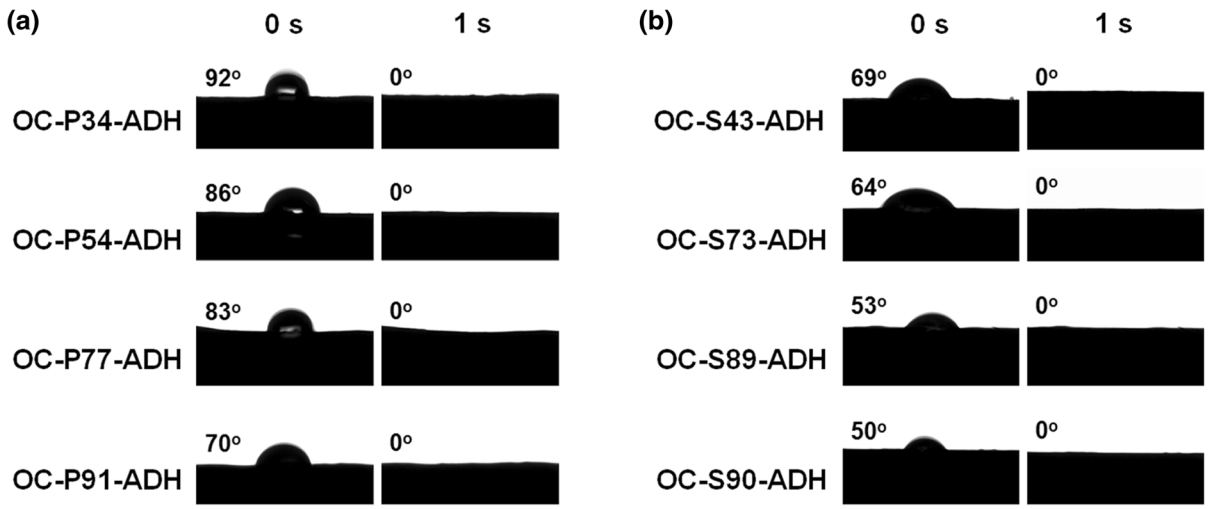

Fig. 7 Water contact angles of the prepared cellulose nanofiber mats

aqueous solution due to the hydrophilicity of cellulose. The pores between these fibers can also absorb aqueous solution based on capillary forces. As shown in Fig. 8a, the water uptake ability of OC-P-ADH fiber mats is affected by the oxidation degree of cellulose. OC-P34-ADH nanofibers can absorb 5.3 g/g SBF, while the other three OC-P-ADH nanofibers of higher oxidation degree can absorb around 7.5 g/g SBF, perhaps due to their higher hydrophilicity as indicated by the above contact angle results (Fig. 7). As the oxidation degree increased from 34 to 91%, the amount of SBF absorbed by the pores between the fibers gradually increased from 5.7 to 17.4 g/g. This is possibly because that both the hydrophilicity and the porosity of the mat increased with the increase of oxidation (Figs. 7 and 3c). The total water uptake ranges between 11.0 and 25.6 g/g.

The OC-S-ADH nanofiber mats can absorb 30.0 g/g SBF, and oxidation degree exhibits no significant effects. The water uptake ability of OC-S-ADH nanofibers is 6.7 g/g, which is comparable to that of OC-P-ADH nanofibers. By contrast, the pores between OC-S-ADH nanofibers can absorb 24.0 g/g SBF, which is 1.2–2.7 times higher than that of OC-P-ADH fiber mats. The higher water uptake ability of OC-S-ADH nanofiber mats than OC-P-ADH nanofiber mats corresponds to the higher hydrophilicity of the former than that of the latter (Fig. 7).

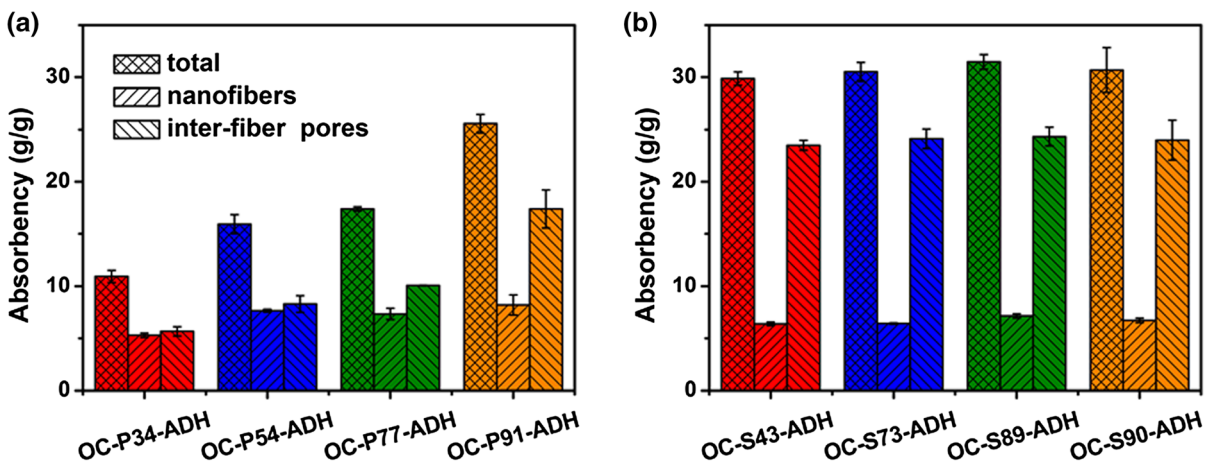

Fig. 8 The water uptake ability of the cellulose nanofiber mats

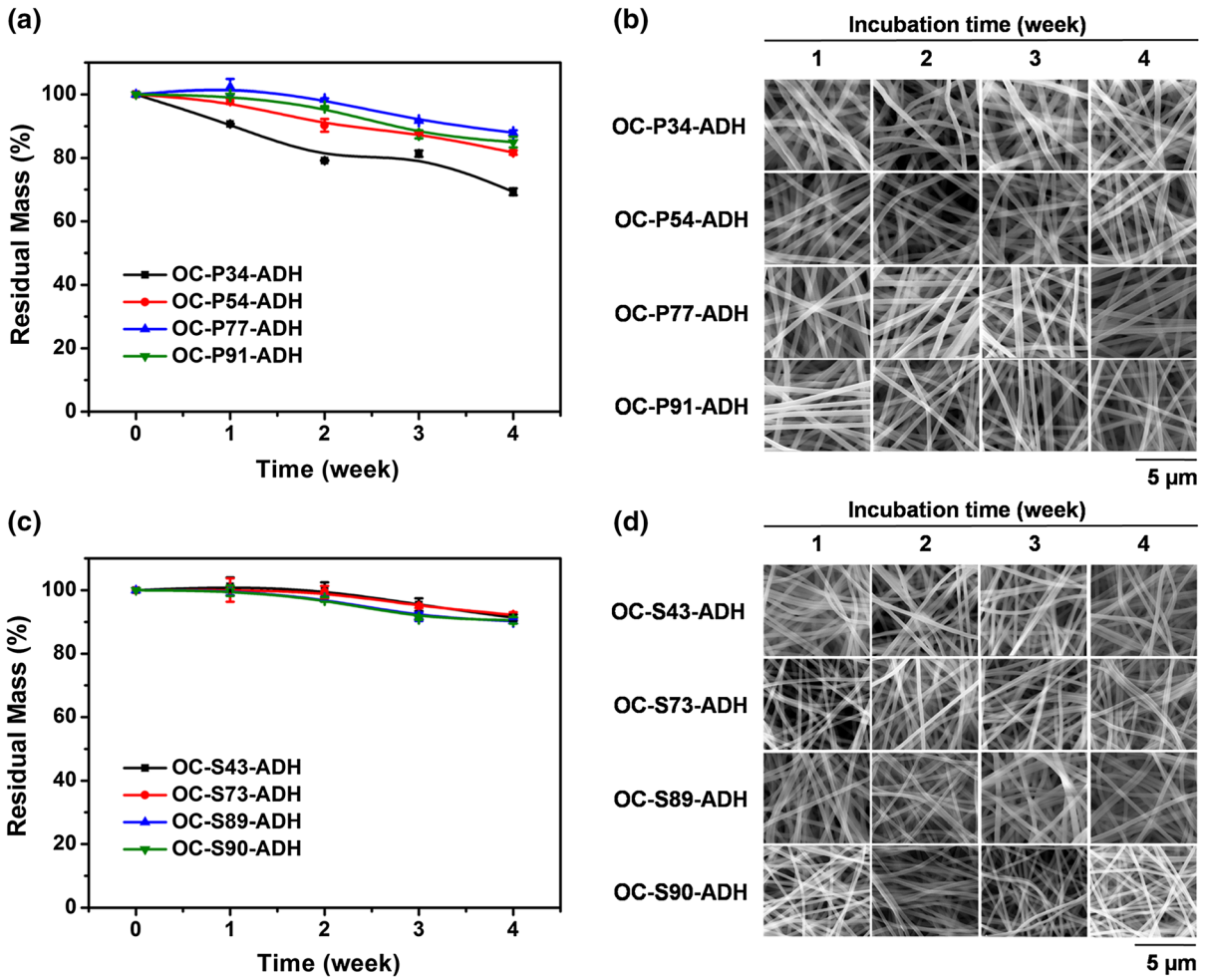

Fig. 9 Mass (**a**, **c**) and morphology (**b**, **d**) change profiles of the prepared cellulose nanofibers in simulated body fluid at 37 °C

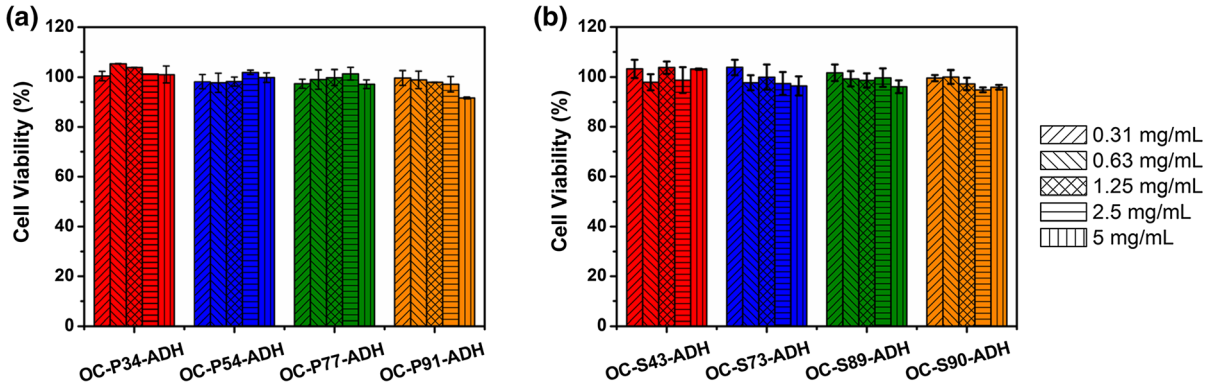

Fig. 10 Viability of L929 fibroblast cells cultured in the leachates of the prepared cellulose nanofibers

In summary, the ADH-crosslinked OC nanofiber mats are capable of absorbing up to 30.0 g/g SBF. As wound dressings, they can absorb excess wound exudates, preventing maceration of the surrounding normal skin and maintaining a favorable moist healing environment for wounds (Mihai et al. 2019; Sweeney et al. 2012). As tissue engineering scaffolds, the mats can hold a large amount of water, forming a highly hydrated environment mimicking natural extracellular matrix, benefiting cell growth (Chakraborty et al. 2019). The mats when used as drug carriers can facilitate the release of some hydrophobic drugs and enhance their absorption by body (Ravikumar et al. 2017; Yu et al. 2012).

Degradability

Our control experiments showed that all the as-spun OC nanofibers have very poor water resistance, and they could completely dissolve in SBF in a few minutes. In comparison, all the ADH-crosslinked OC nanofibers have good water resistance and they degraded in SBF gradually. The morphology and mass loss of the crosslinked cellulose nanofibers in SBF are shown in Fig. 9. OC-P34-ADH nanofibers degraded fastest. After 4 weeks, they lost more than 30% of their initial mass. OC-P77-ADH nanofibers degraded the slowest. They lost only 12% of their initial mass after 4 weeks. OC-S-ADH nanofibers degraded slower than OC-P-ADH nanofibers. All OC-S-ADH fibers degraded very slowly and oxidation degree of had little effect on the degradation rate. After 4 weeks, they only lost 10% of their initial mass. All fibers retained good nanofibrous morphologies during the degradation process (Fig. 9b, d). These results indicate that the crosslinked OC nanofibers are degradable. Biomaterials used in the body should degrade and be cleared from the body after completing their functions. The degradability of OC-ADH nanofibers is beneficial for in vivo biomedical applications. In addition, the kidneys are only able to clear macromolecules with molecular weight lower than 50 kDa. Macromolecules of higher molecular weight are not able to be cleared from body, thus may undergo bioaccumulation and cause macromolecular syndrome (DeMerlis and Schoneker 2003). OC-S and OC-P samples have molecular weights below 5600 Da (Fig. 1). When used in vivo, ADH-crosslinked OC nanofibers may undergo hydrolysis of β-glycosidic bonds or imine crosslinking bonds (Lee et al. 2000), releasing molecular chain fragments. The fragments of this small size might easily be eliminated by the kidneys.

Biocompatibility

Figure 10 shows the viability of L929 fibroblast cells cultured in the medium containing the leachates of ADH-crosslinked OC fibers for 24 h. Cells cultured in blank medium were used as positive controls. For all the OC-ADH fibers, the cell viability kept over 90% at all tested concentrations, suggesting good biocompatibility of these fibers. In the crosslinking process, the crosslinking reagent must enter the interior of the nanofibers and is difficult to remove completely after crosslinking. Therefore, the toxic crosslinking reagent may cause toxicity to the crosslinked fibers. This has been seen for the generally used crosslinking reagent glutaraldehyde in our previous studies (Lv et al. 2019; Zhang et al. 2019). Here, we used ADH as the crosslinking reagent for OC nanofibers. ADH is not a hazardous substance as classified by the Globally Harmonized System of Classification and Labelling of Chemicals. The good biocompatibility of the ADH-crosslinked OC nanofibers demonstrates that ADH did not introduce toxicity to the fibers, probably due to its non-/low toxicity. The ADH-crosslinked OC nanofibers have good biocompatibility and thus are safe for biomedical applications.

Conclusion

Cellulose nanofibers were prepared with the periodate oxidation—ADH crosslinking strategy, without using unfavorable organic solvents. The cellulose nanofibers showed moderate mechanical strength, excellent water absorbency, enhanced degradability, and good biocompatibility, and are expected to find applications in biomedical fields such as wound healing and tissue regeneration.

Acknowledgments This work was supported by the Fundamental Research Funds for the Central Universities (Nos. 2412019FZ041, 2412019FZ024) and the National Natural Science Foundation of China (No. 51732003).

References

Chakraborty PK, Adhikari J, Saha P (2019) Facile fabrication of electrospun regenerated cellulose nanofiber scaffold for potential bone-tissue engineering application. Int J Biol Macromol 122:644–652. https://doi.org/10.1016/j.ijbiomac.2018.10.216

Chen S, Cui S, Zhang H et al (2018) Cross-linked pectin nanofibers with enhanced cell adhesion. Biomacromol 19:490–498. https://doi.org/10.1021/acs.biomac.7b01605

Cullen B, Watt PW, Lundqvist C et al (2002) The role of oxidised regenerated cellulose/collagen in chronic wound repair and its potential mechanism of action. Int J Biochem Cell B 34:1544–1556. https://doi.org/10.1016/S1357-2725(02)00054-7

DeMerlis CC, Schoneker DR (2003) Review of the oral toxicity of polyvinyl alcohol (PVA). Food Chem Toxicol 41:319–326. https://doi.org/10.1016/S0278-6915(02)00258-2

Dong J, Ghiladi RA, Wang Q et al (2018) Protoporphyrin-IX conjugated cellulose nanofibers that exhibit high antibacterial photodynamic inactivation efficacy. Nanotechnology 29:265601. https://doi.org/10.1088/1361-6528/aabb3c

Du J, Hsieh YL (2009) Cellulose/chitosan hybrid nanofibers from electrospinning of their ester derivatives. Cellulose 16:247–260. https://doi.org/10.1007/s10570-008-9266-9

Fan QG, Lewis DM, Tapley KN (2001) Characterization of cellulose aldehyde using Fourier transform infrared spectroscopy. J Appl Polym Sci 82:1195–1202. https://doi.org/10.1002/app.1953

French AD (2014) Idealized powder diffraction patterns for cellulose polymorphs. Cellulose 21:885–896. https://doi.org/10.1007/s10570-013-0030-4

Frenot A, Henriksson MW, Walkenström P (2007) Electrospinning of cellulose-based nanofibers. J Appl Polym Sci 103:1473–1482. https://doi.org/10.1002/app.24912

Frey MW (2008) Electrospinning cellulose and cellulose derivatives. Polym Rev 48:378–391. https://doi.org/10.1080/15583720802022281

Gabriel A, Barrett C, Cullen B et al (2020) Infection and inflammation in the wound environment: addressing issues of delayed wound healing with advanced wound dressings. Wounds 32:S1–S17

Han SO, Youk JH, Min KD et al (2008) Electrospinning of cellulose acetate nanofibers using a mixed solvent of acetic acid/water: effects of solvent composition on the fiber diameter. Mater Lett 62:759–762. https://doi.org/10.1016/j.matlet.2007.06.059

Hart J, Silcock D, Gunnigle S et al (2002) The role of oxidised regenerated cellulose/collagen in wound repair: effects in vitro on fibroblast biology and in vivo in a model of compromised healing. Int J Biochem Cell B 34:1557–1570. https://doi.org/10.1016/S1357-2725(02)00062-6

Hou L, Udangawa WMRN, Pochiraju A et al (2016) Synthesis of heparin-immobilized, magnetically addressable cellulose nanofibers for biomedical applications. ACS Biomater Sci Eng 2:1905–1913. https://doi.org/10.1021/acsbiomaterials.6b00273

Huang ZM, Zhang YZ, Kotaki M et al (2003) A review on polymer nanofibers by electrospinning and their applications in nanocomposites. Compos Sci Technol 63:2223–2253. https://doi.org/10.1016/S0266-3538(03)00178-7

Kenawy E-R, Bowlin GL, Mansfield K et al (2002) Release of tetracycline hydrochloride from electrospun poly(-ethylene-co-vinylacetate), poly(lactic acid), and a blend. J Controlled Release 81:57–64. https://doi.org/10.1016/S0168-3659(02)00041-X

Khan TA, Peh KK, Ch'ng HS (2000) Mechanical, bioadhesive strength and biological evaluations of chitosan films for wound dressing. J Pharm Pharm Sci 3:303–311

Khil MS, Cha DI, Kim HY et al (2003) Electrospun nanofibrous polyurethane membrane as wound dressing. J Biomed Mater Res B 67B:675–679. https://doi.org/10.1002/jbm.b.10058

Kim CW, Kim DS, Kang SY et al (2006) Structural studies of electrospun cellulose nanofibers. Polymer 47:5097–5107. https://doi.org/10.1016/j.polymer.2006.05.033

Kim UJ, Kuga S, Wada M et al (2000) Periodate oxidation of crystalline cellulose. Biomacromol 1:488–492. https://doi.org/10.1021/bm0000337

Kim UJ, Wada M, Kuga S (2004) Solubilization of dialdehyde cellulose by hot water. Carbohyd Polym 56:7–10. https://doi.org/10.1016/j.carbpol.2003.10.013

Kishan AP, Cosgriff-Hernandez EM (2017) Recent advancements in electrospinning design for tissue engineering applications: a review. J Biomed Mater Res A 105:2892–2905. https://doi.org/10.1002/jbm.a.36124

Klemm D, Kramer F, Moritz S et al (2011) Nanocelluloses: a new family of nature-based materials angewandte chemie. Angew Chem Int Ed 50:5438–5466. https://doi.org/10.1002/anie.201001273

Kulpinski P (2005) Cellulose nanofibers prepared by the N-methylmorpholine-N-oxide method. J Appl Polym Sci 98:1855–1859. https://doi.org/10.1002/app.22123

Lee KY, Bouhadir KH, Mooney DJ (2000) Degradation behavior of covalently cross-linked Poly(aldehyde guluronate) hydrogels. Macromolecules 33:97–101. https://doi.org/10.1021/ma991286z

Leguy J, Diallo A, Putaux J-L et al (2018) Periodate oxidation followed by $NaBH_4$ reduction converts microfibrillated cellulose into sterically stabilized neutral cellulose nanocrystal suspensions. Langmuir 34:11066–11075. https://doi.org/10.1021/acs.langmuir.8b02202

Liu P, Mai C, Zhang K (2017) Formation of uniform multi-stimuli-responsive and multiblock hydrogels from dialdehyde cellulose. ACS Sustain Chem Eng 5:5313–5319. https://doi.org/10.1021/acssuschemeng.7b00646

Lv H, Cui S, Zhang H et al (2019) Crosslinked starch nanofibers with high mechanical strength and excellent water resistance for biomedical applications. Biomed Mater 15:025007. https://doi.org/10.1088/1748-605X/ab509f

Magalhães WLE, Cao X, Lucia LA (2009) Cellulose nanocrystals/cellulose core-in-shell nanocomposite assemblies. Langmuir 25:13250–13257. https://doi.org/10.1021/la901928j

Matthews JA, Wnek GE, Simpson DG et al (2002) Electrospinning of collagen nanofibers. Biomacromol 3:232–238. https://doi.org/10.1021/bm015533u

Mihai MM, Dima BM, Dima B et al (2019) Nanomaterials for wound healing and infection control. Materials 12:2176. https://doi.org/10.3390/ma12132176

Morán JI, Alvarez VA, Cyras VP et al (2008) Extraction of cellulose and preparation of nanocellulose from sisal fibers. Cellulose 15:149–159. https://doi.org/10.1007/s10570-007-9145-9

Münster L, Vícha J, Klofáč J et al (2017) Stability and aging of solubilized dialdehyde cellulose. Cellulose 24:2753–2766. https://doi.org/10.1007/s10570-017-1314-x

Phan DN, Dorjjugder N, Khan MQ et al (2019) Synthesis and attachment of silver and copper nanoparticles on cellulose nanofibers and comparative antibacterial study. Cellulose 26:6629–6640. https://doi.org/10.1007/s10570-019-02542-6

Quan SL, Kang SG, Chin IJ (2010) Characterization of cellulose fibers electrospun using ionic liquid. Cellulose 17:223–230. https://doi.org/10.1007/s10570-009-9386-x

Ravikumar R, Ganesh M, Ubaidulla U et al (2017) Preparation, characterization, and in vitro diffusion study of nonwoven electrospun nanofiber of curcumin-loaded cellulose acetate phthalate polymer. Saudi Pharm J 25:921–926. https://doi.org/10.1016/j.jsps.2017.02.004

Saito T, Isogai A (2004) TEMPO-mediated oxidation of native cellulose. The effect of oxidation conditions on chemical and crystal structures of the water-insoluble fractions. Biomacromol 5:1983–1989. https://doi.org/10.1021/bm0497769

Schiffman JD, Schauer CL (2008) A Review: electrospinning of biopolymer nanofibers and their applications. Polym Rev 48:317–352. https://doi.org/10.1080/15583720802022182

Sweeney IR, Miraftab M, Collyer G (2012) A critical review of modern and emerging absorbent dressings used to treat exuding wounds. Int Wound J 9:601–612. https://doi.org/10.1111/j.1742-481X.2011.00923.x

Vallejos ME, Peresin MS, Rojas OJ (2012) All-cellulose composite fibers obtained by electrospinning dispersions of cellulose acetate and cellulose nanocrystals. J Polym Environ 20:1075–1083. https://doi.org/10.1007/s10924-012-0499-1

Viswanathan G, Murugesan S, Pushparaj V et al (2006) Preparation of biopbolymer fibers by electrospinning from room temperature ionic liquids. Biomacromol 7:415–418. https://doi.org/10.1021/bm050837s

Wu S, Applewhite AJ, Niezgoda J et al (2017) Oxidized regenerated cellulose/collagen dressings: review of evidence and recommendations. Adv Skin Wound Care 30:S1–S18. https://doi.org/10.1097/01.ASW.0000525951.20270.6c

Xu S, Zhang J, He A et al (2008) Electrospinning of native cellulose from nonvolatile solvent system. Polymer 49:2911–2917. https://doi.org/10.1016/j.polymer.2008.04.046

Yan G, Zhang X, Li M et al (2019) Stability of soluble dialdehyde cellulose and the formation of hollow microspheres: optimization and characterization. ACS Sustain Chem Eng 7:2151–2159. https://doi.org/10.1021/acssuschemeng.8b04825

Yu DG, Yu JH, Chen L et al (2012) Modified coaxial electrospinning for the preparation of high-quality ketoprofen-loaded cellulose acetate nanofibers. Carbohyd Polym 90:1016–1023. https://doi.org/10.1016/j.carbpol.2012.06.036

Zaman HU, Islam JMM, Khan MA et al (2011) Physico-mechanical properties of wound dressing material and its biomedical application. J Mech Behav Biomed 4:1369–1375. https://doi.org/10.1016/j.jmbbm.2011.05.007

Zhang H, Cui S, Lv H et al (2019) A crosslinking strategy to make neutral polysaccharide nanofibers robust and biocompatible: with konjac glucomannan as an example. Carbohyd Polym 215:130–136. https://doi.org/10.1016/j.carbpol.2019.03.075